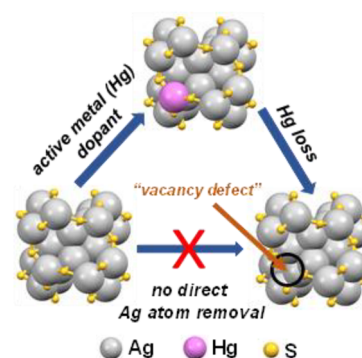


Tailoring Vacancy Defects in Isolated Atomically Precise Silver Clusters through Mercury-Doped Intermediates

Papri Chakraborty,^{*} Sami Malola, Patrick Weis, Marco Neumaier, Erik Karsten Schneider, Hannu Häkkinen,^{*} and Manfred M. Kappes^{*}

ABSTRACT: Vacancy defects are known to have significant effects on the physical and chemical properties of nanomaterials. However, the formation and structural dynamics of vacancy defects in atomically precise coinage metal clusters have hardly been explored due to the challenges associated with isolation of such defected clusters. Herein, we isolate $[\text{Ag}_{28}(\text{BDT})_{12}]^{2-}$ (BDT is 1,3-benzenedithiol), a cluster with a “missing atom” site compared to $[\text{Ag}_{29}(\text{BDT})_{12}]^{3-}$, whose precise structure is known from X-ray diffraction. $[\text{Ag}_{28}(\text{BDT})_{12}]^{2-}$ was formed in the gas-phase by collisional heating of $[\text{Ag}_{28}\text{Hg}(\text{BDT})_{12}]^{2-}$, a Hg-doped analogue of the parent cluster. The structural changes resulting from the loss of the Hg heteroatom were investigated by trapped ion mobility mass spectrometry. Density functional theory calculations were performed to provide further insights into the defect structures, and molecular dynamics simulations revealed defect site-dependent structural relaxation processes.



Exploring the chemistry and self-healing of defects in materials science is an important area of research as defects play significant roles in controlling optical, chemical, mechanical and electronic properties of the system.¹ For example, vacancy defects on the surface of nanomaterials are known to dramatically affect their catalytic properties.^{2,3} Ligand-protected clusters of noble metals make up an emerging class of nanomaterials with unique physical and chemical properties.^{4–9} These clusters are atomically precise, with their structures typically known from single crystal X-ray diffraction. While the effect of introducing dopant atoms as “antisite” point defects on the structure and properties of these clusters has been investigated in detail,^{10,11} the consequences of creating “vacancy site” defects by removing atoms are less well explored. Hollow, 12-atom icosahedral metal cores have been observed in the crystal structures of several clusters like $\text{Ag}_{44}(\text{SR})_{30}$, $\text{Au}_{144}(\text{SR})_{60}$, etc. (SR is a thiolate ligand), although filled 13-atom icosahedral cores are expected to be structurally more stable.^{12–14} Zhou et al. have demonstrated that the removal of two kernel Au atoms from $\text{Au}_{48}(\text{SR})_{26}$ by thermally activated solution chemistry has a significant effect on the photoluminescence properties of the resulting cluster.¹⁵ Dong et al. reported well-defined vacancy defects on the surface of ligand-stabilized $\text{Cu}_{36}\text{H}_{10}$ nanoclusters.¹⁶ Such studies based mostly on bottom up synthesis indicate the possibilities of tailoring vacancy defects in atomically precise clusters to study their structure–property correlations in the condensed phase. However, removal of single atoms from preformed clusters to create vacancy sites is thermodynamically quite unfavorable due to their high cohesive energy.¹⁷

This poses significant challenges for the synthesis and isolation of such clusters.

Herein, we characterized $[\text{Ag}_{28}(\text{BDT})_{12}]^{2-}$ (BDT is 1,3-benzene dithiol) in the gas-phase, a cluster with a missing Ag atom site compared to $[\text{Ag}_{29}(\text{BDT})_{12}]^{3-}$ whose molecular structure is precisely known from X-ray crystallography.¹⁸ The vacancy defect was created from a heteroatom (Hg)-doped analogue of $[\text{Ag}_{29}(\text{BDT})_{12}]^{3-}$ to overcome the challenges associated with single Ag atom removal from the homonuclear cluster. First, we introduced Hg, an active metal dopant, into the preformed cluster by solution reaction. This resulted in the formation of $[\text{Ag}_{28}\text{Hg}(\text{BDT})_{12}]^{2-}$, which upon electrospray ionization and subsequent collisional heating led to the efficient loss of the Hg atom and the formation of $[\text{Ag}_{28}(\text{BDT})_{12}]^{2-}$. The isolated $[\text{Ag}_{28}(\text{BDT})_{12}]^{2-}$ fragment species was characterized in the gas-phase using electrospray ionization mass spectrometry (ESI MS) and structural changes upon the loss of the heteroatom was studied through trapped ion mobility spectrometry (TIMS). Possible structures of $[\text{Ag}_{28}(\text{BDT})_{12}]^{2-}$ were investigated by using density functional theory (DFT) calculations. Moreover, molecular dynamics (MD) simulations were performed to understand the dynamic

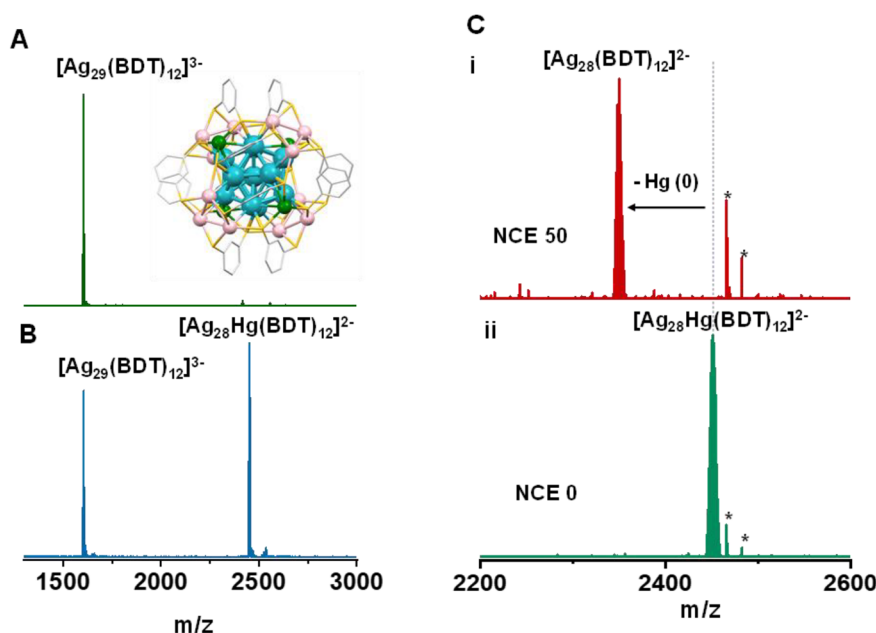


Figure 1. ESI MS of (A) pure $[\text{Ag}_{29}(\text{BDT})_{12}]^{3-}$ cluster, (B) $[\text{Ag}_{28}\text{Hg}(\text{BDT})_{12}]^{2-}$ and $[\text{Ag}_{29}(\text{BDT})_{12}]^{3-}$ mixture, and (C) collision-induced dissociation of $[\text{Ag}_{28}\text{Hg}(\text{BDT})_{12}]^{2-}$ at normalized collision energy (NCE) of (i) 50 and (ii) 0. DFT-optimized structure of $[\text{Ag}_{29}(\text{BDT})_{12}]^{3-}$ (using the coordinates of the crystal structure) is presented in the inset of panel A. Color codes: blue, Ag atoms in icosahedron core of the cluster; pink, Ag atoms of the Ag_3S_3 surface “staple” motifs; green, four Ag atoms at tetrahedral positions on the cluster surface where phosphine ligands are attached in the crystal structure; yellow, S; gray, C. H atoms are not shown for clarity. Peaks marked with an asterisk are electronic artifacts.

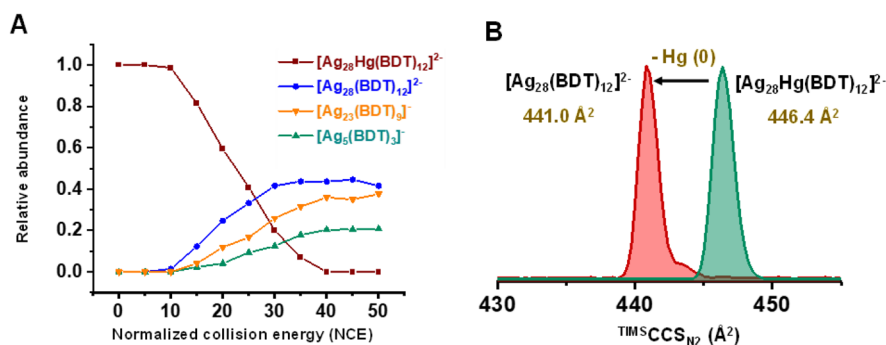


Figure 2. (A) NCE-resolved fragmentation curves of $[\text{Ag}_{28}\text{Hg}(\text{BDT})_{12}]^{2-}$ and (B) TIMS mobilogram of $[\text{Ag}_{28}\text{Hg}(\text{BDT})_{12}]^{2-}$ and $[\text{Ag}_{28}(\text{BDT})_{12}]^{2-}$ cluster.

changes resulting from the creation of a vacancy defect in the cluster.

The $[\text{Ag}_{29}(\text{BDT})_{12}(\text{TPP})_4]^{3-}$ (TPP is triphenyl phosphine) cluster was synthesized following a reported method¹⁸ and characterized using ESI MS as shown in Figure 1A. The mass spectrum showed a dominant peak at m/z 1603 corresponding to $[\text{Ag}_{29}(\text{BDT})_{12}]^{3-}$. The known crystal structure of the cluster is presented in the inset of Figure 1A. The cluster consists of four distinct types of silver atoms: (1) the central Ag atom of the icosahedral core, (2) the 12 equivalent positions on the icosahedral shell, (3) the four Ag atoms at tetrahedral positions on the surface to which TPP ligands are bound in the condensed phase structure but lost during electrospray ionization,^{19,20} and (4) the 12 Ag atoms comprising the four Ag_3S_3 motifs on the surface. So, it is possible, in principle, that a heteroatom would be doped in any of these four possible positions in the cluster.

We reacted the cluster with $\text{Hg}(\text{OAc})_2$ and $[\text{Ag}_{28}\text{Hg}(\text{BDT})_{12}]^{2-}$ was formed as the product, which was characterized by ESI MS (peak at m/z 2452, see Figure 1B).

The conversion of $[\text{Ag}_{29}(\text{BDT})_{12}]^{3-}$ to $[\text{Ag}_{28}\text{Hg}(\text{BDT})_{12}]^{2-}$ was dependent on the amount of $\text{Hg}(\text{OAc})_2$ used in the reaction (Figure S1). The relative abundance of the doped product $[\text{Ag}_{28}\text{Hg}(\text{BDT})_{12}]^{2-}$ increased as the concentration of $\text{Hg}(\text{OAc})_2$ (30–80 μM) added to the cluster (3 μM) increased. However, at a further higher concentration of $\text{Hg}(\text{OAc})_2$, degradation of the cluster was observed (Figure S1A). In particular, no higher amount of Hg doping was observed, which can be realized from the absence of any peak for $[\text{Ag}_{27}\text{Hg}_2(\text{BDT})_{12}]^{1-}$ (expected m/z 4996) in ESI MS (Figure S1). The experimental and calculated isotopic distributions of the peaks (Figure S2) and changes in optical absorption spectra (Figure S3) are presented in the Supporting Information. Broadening of the peak at 447 nm was observed in optical absorption (Figure S3). Moreover, time-dependent UV-vis (Figure S4) showed no significant change in the minute time scale, and time-dependent ESI MS (Figure S5) showed that the abundance of $[\text{Ag}_{29}(\text{BDT})_{12}]^{3-}$ and $[\text{Ag}_{28}\text{Hg}(\text{BDT})_{12}]^{2-}$ remained almost unchanged with time. This revealed that at room temperature, the reaction reaches

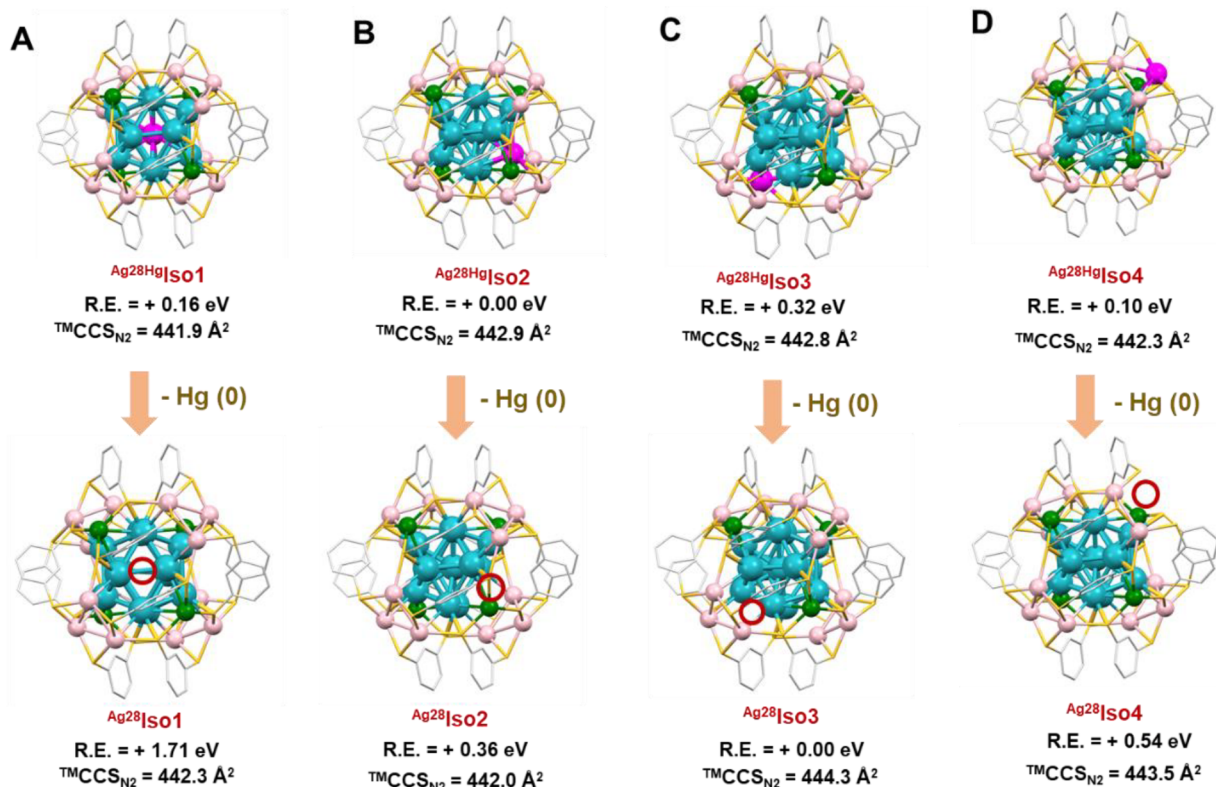
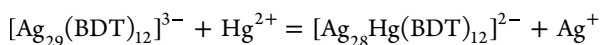


Figure 3. DFT optimized structures of $[Ag_{28}Hg(BDT)_{12}]^{2-}$ considering doping of the Hg atom in four different positions (A) center of the icosahedron, (B) surface of icosahedron, (C) at one of the tetrahedral positions on the surface and (D) on the Ag_3S_3 surface “staple” motifs of the cluster. Structures of $[Ag_{28}(BDT)_{12}]^{2-}$ formed by removal of the Hg atom in each case is shown. The vacant atom sites are indicated by red circles. Color codes: blue, Ag atoms in icosahedron core of the cluster; pink, Ag atoms of the Ag_3S_3 surface “staple” motifs; green, four Ag atoms at tetrahedral positions on the cluster surface; purple, Hg; yellow, S; gray, C. H atoms are not shown for clarity.

equilibrium very rapidly (compared to our instrumental transfer time of ca. 1 min). The doping of Hg into $[Ag_{29}(BDT)_{12}]^{3-}$ in solution presumably occurs by an antihalvanic reduction pathway where Hg^{2+} is first reduced by the cluster and subsequently Hg is doped into the cluster. The proposed reaction pathway is as follows:



Analogous doping by Hg atoms in solution has previously been observed in case of $[Au_{25}(SR)_{18}]^-$ where the X-ray structure resolved Hg in the outer shell positions of the cluster.^{21,22} Note that doping of heteroatoms into coinage metal clusters is known to affect their properties and applications,^{10,11,23} and similar behavior is expected also in the case of $[Ag_{29}(BDT)_{12}]^{3-}$. These are specific to the nature of the dopant atom, and a brief comparison of the Hg doping vs doping with other metal atoms (Au, Cu, Pt)^{19,23,24} in $[Ag_{29}(BDT)_{12}]^{3-}$ is discussed in the [Supporting Information](#).

Collisional activation of $[Ag_{28}Hg(BDT)_{12}]^{2-}$ resulted in the efficient loss of the Hg atom and formation of $[Ag_{28}(BDT)_{12}]^{2-}$, as shown in [Figure 1C](#). The loss of neutral Hg (0) can be inferred from the unchanged charge states ($2-$) of $[Ag_{28}Hg(BDT)_{12}]^{2-}$ and $[Ag_{28}(BDT)_{12}]^{2-}$ clusters. Typical CID spectra at varying normalized collision energies (NCE) are presented in [Figure S6](#). Following the removal of the Hg atom, the same fragmentation channel as observed for the reference $[Ag_{29}(BDT)_{12}]^{3-}$ cluster,^{25,26} i.e., $[Ag_5(BDT)_3]^-$ loss, was seen ([Figure S6](#)). The corresponding NCE-resolved fragmentation curves are presented in [Figure 2A](#). Such selective

loss of the heteroatom during collisional activation was not observed in analogous doped clusters such as $[Ag_{28}Au(BDT)_{12}]^{3-}$ ([Figure S7](#)) where Au was retained in the larger fragment as $[Ag_{23}Au(BDT)_9]^{2-}$. In contrast to that, for the Cu-doped analogue of the cluster, $[Ag_{28}Cu(BDT)_{12}]^{3-}$, Cu was retained in the fragments as $[Ag_4Cu(BDT)_3]^-$ and $[Ag_{23}Cu(BDT)_9]^{2-}$.²⁴

The removal of a single atom from the cluster will result in a vacancy defect site, which may affect its overall structural constitution. To explore the structural changes, we performed TIMS studies on isolated $[Ag_{28}Hg(BDT)_{12}]^{2-}$ and $[Ag_{28}(BDT)_{12}]^{2-}$ clusters to obtain collision cross sections (CCS) of the ions in N_2 gas and hence information on the structure.²⁷ The fragment ion was produced by increasing the ion transmission voltages before the TIMS separation ([Figure S8](#)) following previously established methodologies.^{26,28} Respective TIMS mobilograms of parent $[Ag_{28}Hg(BDT)_{12}]^{2-}$ and fragment $[Ag_{28}(BDT)_{12}]^{2-}$ are in [Figure 2B](#). The experimental CCS obtained from TIMS ($^{TIMS}CCS_{N_2}$) of $[Ag_{28}Hg(BDT)_{12}]^{2-}$ and $[Ag_{28}(BDT)_{12}]^{2-}$ were 446.4 \AA^2 and 441.0 \AA^2 , respectively. Thus, TIMS studies revealed a slight contraction (1.2%) in the structure upon removal of the Hg atom. The $^{TIMS}CCS_{N_2}$ resolution achieved for these ions was ~ 200 , and this slight relative change of 1.2% is well above the resolution limit. Also, there was no indication of a second isomer with $>5\%$ relative intensity within this limit of resolution.

To understand the structural changes upon fragmentation, we first computed possible structures of the $[Ag_{28}Hg-$

(BDT)₁₂]²⁻ parent ion considering doping of Hg in four possible sites (as discussed above) of the [Ag₂₉(BDT)₁₂]³⁻ precursor (Figure S9A further clarifies the four possible sites). DFT optimized structures (retaining staple connectivity) are shown in Figure 3. In the energetically lowest structure of [Ag₂₈Hg(BDT)₁₂]²⁻, Hg occupies the icosahedral shell position (^{Ag28}HgIso2, Figure 3B). The nearest neighbor Hg–Ag bonds on the surface of the icosahedron in the best ^{Ag28}HgIso2 are in range 2.86–3.29 Å, while in [Ag₂₉(BDT)₁₂]³⁻ cluster, the corresponding Ag–Ag distances are in range 2.85–3.15 Å, which gives on average an increase of 2%. The bond distance to the central Ag atom increases only slightly from 2.84 to 2.85 Å by 0.3% and to the sulfur from 2.52 to 2.59 Å by 2.7%. The bonds are visualized in Figure S10A. Compared to [Ag₂₉(BDT)₁₂]³⁻, a local expansion of the structure in the Hg-doped cluster is seen, but overall the structure remains essentially the same. We note, however, that all four of the [Ag₂₈Hg(BDT)₁₂]²⁻ isomers considered were within 0.32 eV in energy, suggesting that Hg occupancy in the other sites cannot entirely be ruled out.

Next, starting structures for [Ag₂₈(BDT)₁₂]²⁻ were constructed by removing Hg from each of the four isomers of [Ag₂₈Hg(BDT)₁₂]²⁻ and reoptimizing by DFT (Figure 3). Creating a vacancy at the tetrahedral position ^{Ag28}Iso3 is the most favorable. The other isomers that have their vacancy either at the surface of the icosahedral core or at the Ag₃S₃ surface motifs are +0.36 eV and +0.54 eV higher in energy. A vacancy at the center of the metal core is least probable, being +1.71 eV higher in energy compared to ^{Ag28}Iso3. The structure of the Ag₂₈ core only (without the ligands) is also presented in Figure S9B to clearly represent the difference in the vacant sites of the ^{Ag28}Iso1–4 isomers. For the lowest energy ^{Ag28}Iso3 isomer, the effect of the vacancy on the metal ligand interface is best seen by looking at the Ag–S bonds that lie next to the vacancy site connecting the tetrahedral and Ag₃S₃ metal–ligand surface motifs. These bonds contract on average by 4.8% (from 2.69 to 2.56 Å) due to the vacancy as compared to the intact [Ag₂₉(BDT)₁₂]³⁻ cluster. Ag–S bond distances to the metal core also get shorter by 2.5% from 2.53 to 2.47 Å. These bonds around the vacancy site are highlighted in Figure S10B. The effect is very local, and the changes elsewhere in the structure are subtle.

If ^{Ag28}Iso3, the product predicted to be most stable is formed, the calculated fragmentation energies for the loss of an Hg atom ([Ag₂₈Hg(BDT)₁₂]²⁻ → [Ag₂₈(BDT)₁₂]²⁻ + Hg) lie in the range of ~0.86–1.19 eV, depending on which ^{Ag28}HgIso1–4 is assumed to be the parent. Note that although the fragmentation energies of the four different isomers are within 0.33 eV, activation barriers of the respective processes are expected to be very different. For example, removing Hg from the center of the cluster would involve first transferring the dopant to the surface before detachment.

CCSs of these calculated structures (TMCCS_{N2}) were modeled using the trajectory method (TM) as implemented in IMoS 1.09.²⁹ In our previous report, we discussed the reliability of the calculation method by comparison of the experimental CCS value (476 Å²) of [Ag₂₉(BDT)₁₂]³⁻ to the theoretical CCS based on its crystal structure.²⁶ Note that the lower CCS of [Ag₂₈Hg(BDT)₁₂]²⁻ compared to that of parent [Ag₂₉(BDT)₁₂]³⁻ cluster is primarily associated with the change in its charge state and not the geometrical structure as the charge-induced dipole interactions also effect the CCS.³⁰ TMCCS_{N2} of [Ag₂₈Hg(BDT)₁₂]²⁻ isomers were ~441.9–442.9

Å² in agreement with the experimental value of 446.4 Å². No significant decrease in TMCCS_{N2} was found for the calculated isomers of [Ag₂₈(BDT)₁₂]²⁻ compared to those calculated for [Ag₂₈Hg(BDT)₁₂]²⁻. In the experiment, [Ag₂₈(BDT)₁₂]²⁻ is 1.2% smaller than [Ag₂₈Hg(BDT)₁₂]²⁻. We regard this overall 1–2% level of agreement between experiment and our structural models as excellent, particularly given that IMoS so far uses the general Lennard-Jones parameters for Ag and Hg atoms, which makes the corresponding TMCCS_{N2} simulations subject to larger errors than for molecules containing only lighter elements. A vacancy defect at the previous site of the Hg atom in [Ag₂₈Hg(BDT)₁₂]²⁻ therefore provides a good description of the [Ag₂₈(BDT)₁₂]²⁻ structure, but on the basis of TMCCS_{N2} alone, we cannot decide which of the four possible vacancy defect(s) actually form(s).

To better understand the structural stability of vacancy sites at finite temperatures, we also performed MD simulations on [Ag₂₈(BDT)₁₂]²⁻. A MD simulation (at roughly 290 K) on ^{Ag28}Iso1 with a hollow icosahedron starting structure is presented in Figure 4. Structural changes with time of

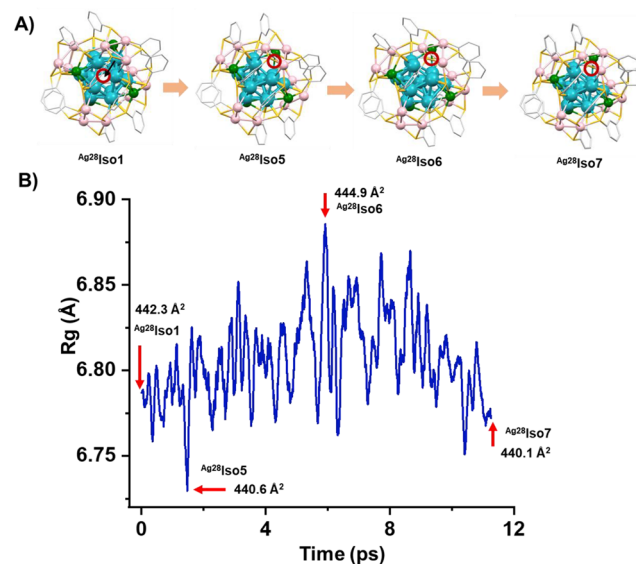


Figure 4. MD simulation on [Ag₂₈(BDT)₁₂]²⁻ cluster (^{Ag28}Iso1): (A) structural changes during the MD simulation at roughly the same cluster orientation and (B) the variation of radius of gyration (Rg) with time of simulation (ps). The vacant atom sites are indicated by red circles, and movement of the Ag atom is marked by an arrow. Color codes: blue, Ag atoms in icosahedron core of the cluster; pink, Ag atoms of the Ag₃S₃ surface “staple” motifs; green, four Ag atoms at tetrahedral positions on the cluster surface; yellow, S; gray, C. H atoms are not shown for clarity.

simulation are reflected in the changes in radius of gyration (Rg) and by several snapshots at intermediate times, as indicated. The data include thermalization from 0 to 3 ps and annealing for 2 ps at the end of the run. During the simulation, it was observed that an Ag atom from the icosahedron shell rapidly migrates to the hollow site at the cluster center and correspondingly the vacancy site migrates to the icosahedron surface, as shown in Figure 4A. The snapshots show that following this, the vacancy in the icosahedral shell then hardly moves on the 12 ps time scale. Only slight changes (±0.1 Å) in size (Rg) of the cluster were observed with time of simulation as shown in Figure 4B. For some of the snapshot structures

from the MD run, we calculated ${}^{\text{TM}}\text{CCS}_{\text{N}_2}$ (Figure S11) and a slight contraction in ${}^{\text{TM}}\text{CCS}_{\text{N}_2}$ was observed in $\text{Ag}^{28}\text{Iso5}$ (440.6 Å² which is 0.5% smaller than $\text{Ag}^{28}\text{HgT Iso3}$) and $\text{Ag}^{28}\text{Iso7}$ (440.1 Å² which is 0.6% smaller than $\text{Ag}^{28}\text{HgT Iso3}$) (Figure 4). Similar fluctuations in Rg ($\pm 1.5\%$) and hence ${}^{\text{TM}}\text{CCS}_{\text{N}_2}$ were also observed during MD simulation (at 278 K) on $\text{Ag}^{28}\text{Iso3}$ (Figure S12). Again, the location of the (tetrahedral) vacancy site remains essentially invariant over the simulation time. The relative energies and ${}^{\text{TM}}\text{CCS}_{\text{N}_2}$ of the possible isomers of $[\text{Ag}_{28}(\text{BDT})_{12}]^{2-}$ are listed in Table S1. We therefore conclude from our MD simulations that at room temperature, core vacancies would rapidly anneal and are therefore unlikely to form in this system, whereas surface vacancies are stable over significantly longer time scales (during which they do not interconvert). In future experimental work, it will be interesting to study to what extent the chemical reactivity of $[\text{Ag}_{28}(\text{BDT})_{12}]^{2-}$ is influenced by such defects.

In summary, we report substitution of a Hg atom into $[\text{Ag}_{29}(\text{BDT})_{12}]^{3-}$ and demonstrate that the resulting doped $[\text{Ag}_{28}\text{Hg}(\text{BDT})_{12}]^{2-}$ cluster forms $[\text{Ag}_{28}(\text{BDT})_{12}]^{2-}$ upon collisional activation in gas phase. The selective loss of the Hg atom results in a vacancy site, which slightly but measurably contracts the overall cluster as measured by its CCS. DFT calculations show that the contraction is seen mainly locally around the vacancy site. We have also used MD simulations to probe associated finite temperature effects. These indicate that at room temperature, migration of Ag atoms surrounding a hypothetical vacancy at the center of the cluster (to form a corresponding surface vacancy) would be almost instantaneous. By contrast, surface vacancies appear significantly longer lived against interconversion. In the future, it will be of interest to synthesize and isolate such clusters with vacancy defects in the condensed phase, which may be attained through thermal treatment on preformed Hg-doped silver clusters and observing the condensed-phase structures of $[\text{Ag}_{28}\text{Hg}(\text{BDT})_{12}]^{2-}$ and $[\text{Ag}_{28}(\text{BDT})_{12}]^{2-}$ by single crystal X-ray diffraction. It will also be of interest to study the effect of such defects on the reactivity and condensed phase properties of these cluster materials.

AUTHOR INFORMATION

Corresponding Authors

Papri Chakraborty – Institute of Nanotechnology, Karlsruhe Institute of Technology, 76344 Eggenstein-Leopoldshafen, Germany; Institute of Physical Chemistry, Karlsruhe Institute of Technology, 76131 Karlsruhe, Germany; orcid.org/0000-0002-1353-7734; Email: pc.paprichakraborty@gmail.com

Hannu Häkkinen – Department of Physics, Nanoscience Center and Department of Chemistry, Nanoscience Center, University of Jyväskylä, 40014 Jyväskylä, Finland; orcid.org/0000-0002-8558-5436; Email: hannu.j.hakkinen@jyu.fi

Manfred M. Kappes – Institute of Nanotechnology, Karlsruhe Institute of Technology, 76344 Eggenstein-Leopoldshafen, Germany; Institute of Physical Chemistry, Karlsruhe Institute of Technology, 76131 Karlsruhe, Germany; orcid.org/0000-0002-1199-1730; Email: manfred.kappes@kit.edu

Authors

Sami Malola – Department of Physics, Nanoscience Center, University of Jyväskylä, 40014 Jyväskylä, Finland

Patrick Weis – Institute of Physical Chemistry, Karlsruhe Institute of Technology, 76131 Karlsruhe, Germany; orcid.org/0000-0001-7006-6759

Marco Neumaier – Institute of Nanotechnology, Karlsruhe Institute of Technology, 76344 Eggenstein-Leopoldshafen, Germany; orcid.org/0000-0002-3810-3377

Erik Karsten Schneider – Institute of Physical Chemistry, Karlsruhe Institute of Technology, 76131 Karlsruhe, Germany

Notes

The authors declare no competing financial interest.

ACKNOWLEDGMENTS

This research was supported by DFG under CRC1441 TrackAct, Project A2. P.C. gratefully acknowledges postdoctoral fellowship support by the Alexander von Humboldt Foundation. P.C. also thanks the Karlsruhe Institute of Technology for providing the guest scientist fellowship during the initial stages of the work. H.H. acknowledges support by the Academy of Finland under grant 315549.

REFERENCES

- (1) Kroger, F. A. Defect Chemistry in Crystalline Solids. *Annu. Rev. Mater. Sci.* **1977**, *7*, 449–475.
- (2) Wang, X.; Zhang, Y.; Si, H.; Zhang, Q.; Wu, J.; Gao, L.; Wei, X.; Sun, Y.; Liao, Q.; Zhang, Z.; et al. Single-Atom Vacancy Defect to Trigger High-Efficiency Hydrogen Evolution of MoS₂. *J. Am. Chem. Soc.* **2020**, *142*, 4298–4308.
- (3) Jia, Y.; Jiang, K.; Wang, H.; Yao, X. The Role of Defect Sites in Nanomaterials for Electrocatalytic Energy Conversion. *Chem.* **2019**, *5*, 1371–1397.
- (4) Chakraborty, I.; Pradeep, T. Atomically Precise Clusters of Noble Metals: Emerging Link between Atoms and Nanoparticles. *Chem. Rev.* **2017**, *117*, 8208–8271.
- (5) Jin, R.; Zeng, C.; Zhou, M.; Chen, Y. Atomically Precise Colloidal Metal Nanoclusters and Nanoparticles: Fundamentals and Opportunities. *Chem. Rev.* **2016**, *116*, 10346–10413.
- (6) Du, Y.; Sheng, H.; Astruc, D.; Zhu, M. Atomically Precise Noble Metal Nanoclusters as Efficient Catalysts: A Bridge between Structure and Properties. *Chem. Rev.* **2020**, *120*, 526–622.
- (7) Aikens, C. M.; Jin, R.; Roy, X.; Tsukuda, T. From Atom-Precise Nanoclusters to Superatom Materials. *J. Chem. Phys.* **2022**, *156*, 170401.
- (8) Biswas, S.; Das, S.; Negishi, Y. Progress and Prospects in the Design of Functional Atomically-Precise Ag(I)-Thiolate Nanoclusters and Their Assembly Approaches. *Coord. Chem. Rev.* **2023**, *492*, 215255.
- (9) Baghdasaryan, A.; Bürgi, T. Copper Nanoclusters: Designed Synthesis, Structural Diversity, and Multiplatform Applications. *Nanoscale* **2021**, *13*, 6283–6340.
- (10) Ghosh, A.; Mohammed, O. F.; Bakr, O. M. Atomic-Level Doping of Metal Clusters. *Acc. Chem. Res.* **2018**, *51*, 3094–3103.

- (11) Khatun, E.; Pradeep, T. New Routes for Multicomponent Atomically Precise Metal Nanoclusters. *ACS Omega* **2021**, *6*, 1–16.
- (12) Kang, X.; Wei, X.; Liu, X.; Wang, S.; Yao, T.; Wang, S.; Zhu, M. A Reasonable Approach for the Generation of Hollow Icosahedral Kernels in Metal Nanoclusters. *Nat. Commun.* **2021**, *12*, 6186.
- (13) Yan, N.; Xia, N.; Liao, L.; Zhu, M.; Jin, F.; Jin, R.; Wu, Z. Unraveling the Long-Pursued Au₁₄₄ Structure by X-Ray Crystallography. *Sci. Adv.* **2018**, *4*, No. eaat7259.
- (14) Desireddy, A.; Conn, B. E.; Guo, J.; Yoon, B.; Barnett, R. N.; Monahan, B. M.; Kirschbaum, K.; Griffith, W. P.; Whetten, R. L.; Landman, U.; et al. Ultrastable Silver Nanoparticles. *Nature* **2013**, *501*, 399–402.
- (15) Zhou, Y.; Liao, L.; Zhuang, S.; Zhao, Y.; Gan, Z.; Gu, W.; Li, J.; Deng, H.; Xia, N.; Wu, Z. Traceless Removal of Two Kernel Atoms in a Gold Nanocluster and Its Impact on Photoluminescence. *Angew. Chem., Int. Ed.* **2021**, *60*, 8668–8672.
- (16) Dong, C.; Huang, R.-W.; Chen, C.; Chen, J.; Nematullov, S.; Guo, X.; Ghosh, A.; Alamer, B.; Hedhili, M. N.; Isimjan, T. T.; et al. [Cu₃₆H₁₀(PET)₂₄(PPh₃)₆Cl₂] Reveals Surface Vacancy Defects in Ligand-Stabilized Metal Nanoclusters. *J. Am. Chem. Soc.* **2021**, *143*, 11026–11035.
- (17) Liu, D.; Zhu, Y. F.; Jiang, Q. Site- and Structure-Dependent Cohesive Energy in Several Ag Clusters. *J. Phys. Chem. C* **2009**, *113*, 10907–10912.
- (18) AbdulHalim, L. G.; Bootharaju, M. S.; Tang, Q.; Del Gobbo, S.; AbdulHalim, R. G.; Eddaoudi, M.; Jiang, D.-e.; Bakr, O. M. Ag₂₉(BDT)₁₂(TPP)₄: A Tetravalent Nanocluster. *J. Am. Chem. Soc.* **2015**, *137*, 11970–11975.
- (19) Soldan, G.; Aljuhani, M. A.; Bootharaju, M. S.; AbdulHalim, L. G.; Parida, M. R.; Emwas, A.-H.; Mohammed, O. F.; Bakr, O. M. Gold Doping of Silver Nanoclusters: A 26-Fold Enhancement in the Luminescence Quantum Yield. *Angew. Chem., Int. Ed.* **2016**, *55*, 5749–5753.
- (20) Chakraborty, P.; Baksi, A.; Mudedla, S. K.; Nag, A.; Paramasivam, G.; Subramanian, V.; Pradeep, T. Understanding Proton Capture and Cation-Induced Dimerization of [Ag₂₉(BDT)₁₂]³⁻ Clusters by Ion Mobility Mass Spectrometry. *Phys. Chem. Chem. Phys.* **2018**, *20*, 7593–7603.
- (21) Yao, C.; Lin, Y.-j.; Yuan, J.; Liao, L.; Zhu, M.; Weng, L.-h.; Yang, J.; Wu, Z. Mono-Cadmium Vs Mono-Mercury Doping of Au₂₅ Nanoclusters. *J. Am. Chem. Soc.* **2015**, *137*, 15350–15353.
- (22) Liao, L.; Zhou, S.; Dai, Y.; Liu, L.; Yao, C.; Fu, C.; Yang, J.; Wu, Z. Mono-Mercury Doping of Au₂₅ and the Homo/Lumo Energies Evaluation Employing Differential Pulse Voltammetry. *J. Am. Chem. Soc.* **2015**, *137*, 9511–9514.
- (23) Bootharaju, M. S.; Kozlov, S. M.; Cao, Z.; Harb, M.; Parida, M. R.; Hedhili, M. N.; Mohammed, O. F.; Bakr, O. M.; Cavallo, L.; Basset, J.-M. Direct Versus Ligand-Exchange Synthesis of [PtAg₂₈(BDT)₁₂(TPP)₄]⁴⁻ Nanoclusters: Effect of a Single-Atom Dopant on the Optoelectronic and Chemical Properties. *Nanoscale* **2017**, *9*, 9529–9536.
- (24) Baksi, A.; Schneider, E. K.; Weis, P.; Chakraborty, I.; Fuhr, O.; Lebedkin, S.; Parak, W. J.; Kappes, M. M. Linear Size Contraction of Ligand Protected Ag₂₉ Clusters by Substituting Ag with Cu. *ACS Nano* **2020**, *14*, 15064–15070.
- (25) Chakraborty, P.; Baksi, A.; Khatun, E.; Nag, A.; Ghosh, A.; Pradeep, T. Dissociation of Gas Phase Ions of Atomically Precise Silver Clusters Reflects Their Solution Phase Stability. *J. Phys. Chem. C* **2017**, *121*, 10971–10981.
- (26) Chakraborty, P.; Malola, S.; Neumaier, M.; Weis, P.; Häkkinen, H.; Kappes, M. M. Elucidating the Structures of Intermediate Fragments During Stepwise Dissociation of Monolayer-Protected Silver Clusters. *Angew. Chem., Int. Ed.* **2023**, *62*, No. e202305836.
- (27) Ridgeway, M. E.; Lubeck, M.; Jordens, J.; Mann, M.; Park, M. A. Trapped Ion Mobility Spectrometry: A Short Review. *Int. J. Mass Spectrom.* **2018**, *425*, 22–35.
- (28) Morsa, D.; Hanozin, E.; Eppe, G.; Quinton, L.; Gabelica, V.; Pauw, E. D. Effective Temperature and Structural Rearrangement in Trapped Ion Mobility Spectrometry. *Anal. Chem.* **2020**, *92*, 4573–4582.
- (29) Larriba, C.; Hogan, C. J., Jr. Ion Mobilities in Diatomic Gases: Measurement Versus Prediction with Non-Specular Scattering Models. *J. Phys. Chem. A* **2013**, *117*, 3887–3901.
- (30) Weis, P.; Hennrich, F.; Fischer, R.; Schneider, E. K.; Neumaier, M.; Kappes, M. M. Probing the Structure of Giant Fullerenes by High Resolution Trapped Ion Mobility Spectrometry. *Phys. Chem. Chem. Phys.* **2019**, *21*, 18877–18892.